Supplementary Figures

Supplementary Figure 1

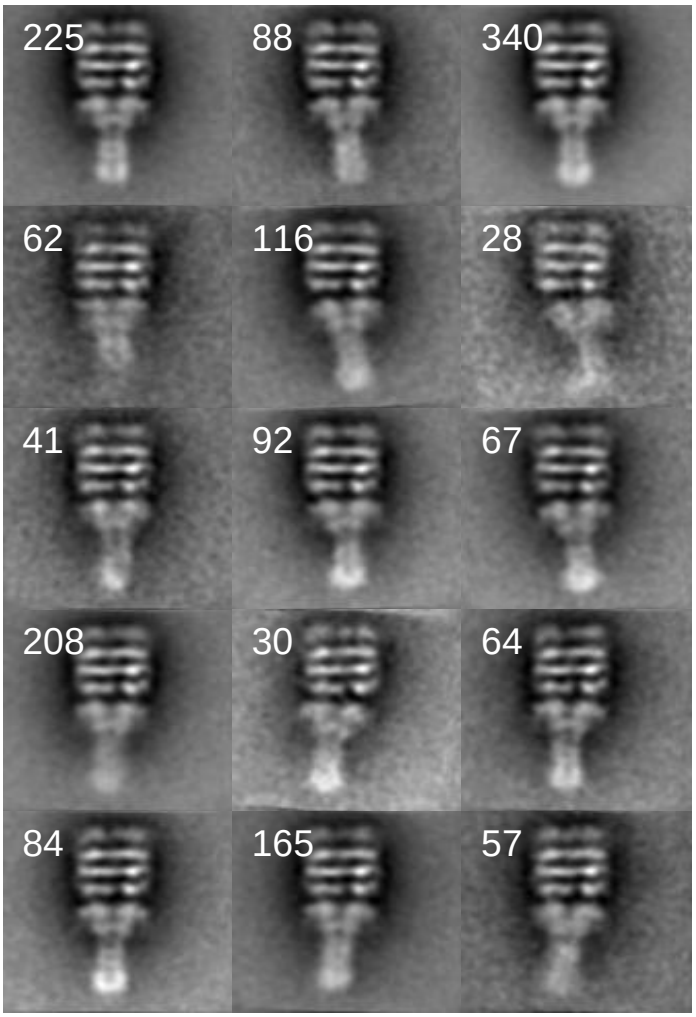

Supplementary Figure 1. Positioning of complex is highly variable. Particles were aligned based on GroEL only and classified based on PA pore. Tilt and shift of PA pore is apparent. Number of particles in each class is shown at upper left corner.

Supplementary Figure 2

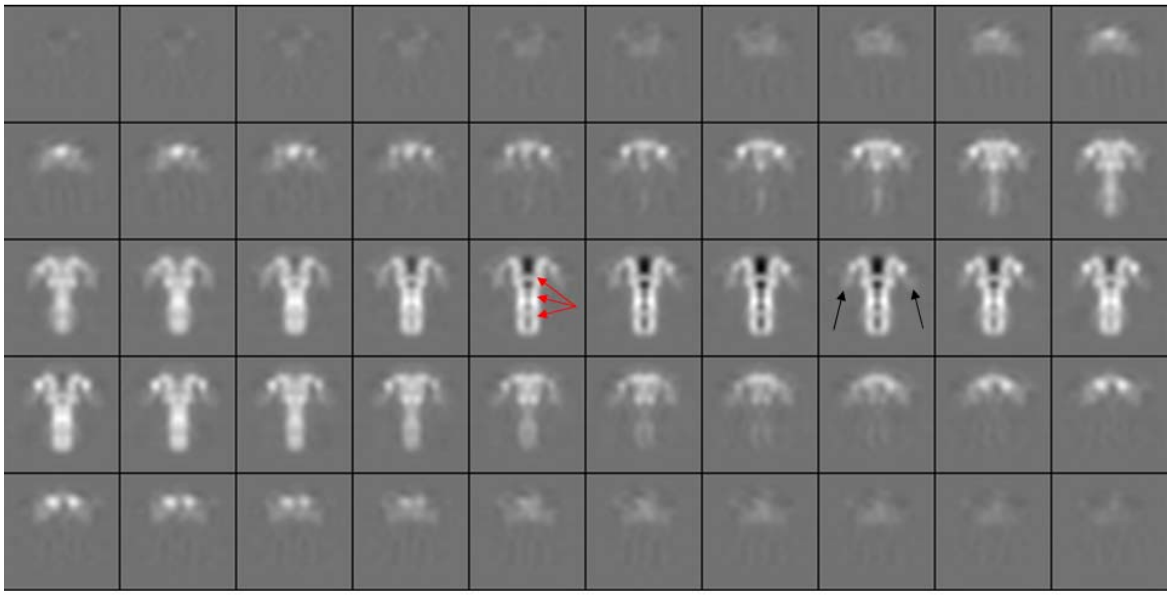

Supplementary Figure 2. Slices of three dimensional reconstruction of PA pore that is bound to GroEL. Red arrows show regions of protein density within the pore channel. Black arrows show the regions contributed from domain 4.

Supplementary Figure 3

(A) GroEL-PA pore complex

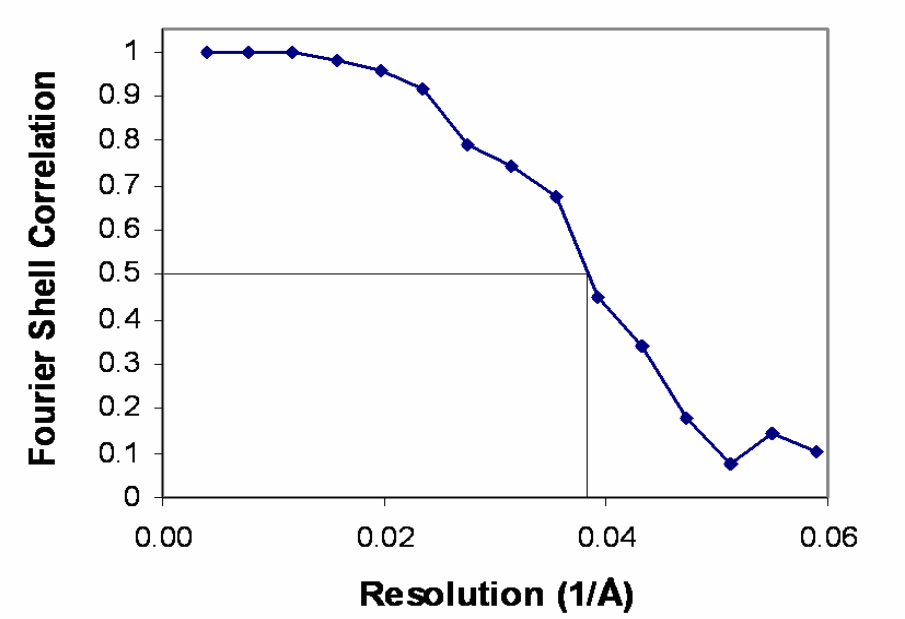

(B) Free PA pore

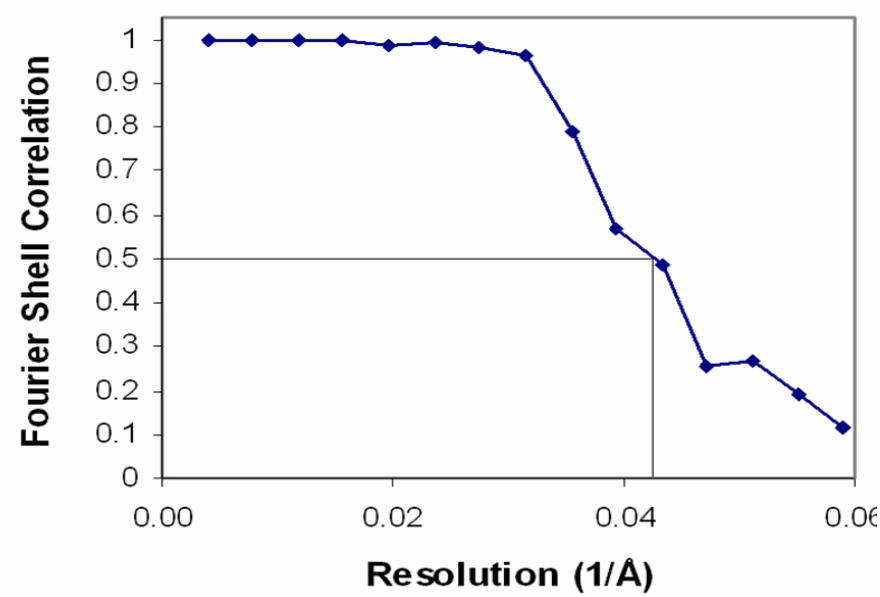

Supplementary Figure 3. (A)Fourier Shell correlation curve of GroEL-bound PA pore reconstruction. (B) Fourier Shell correlation curve of free PA pore reconstruction.

Supplementary Figure 4

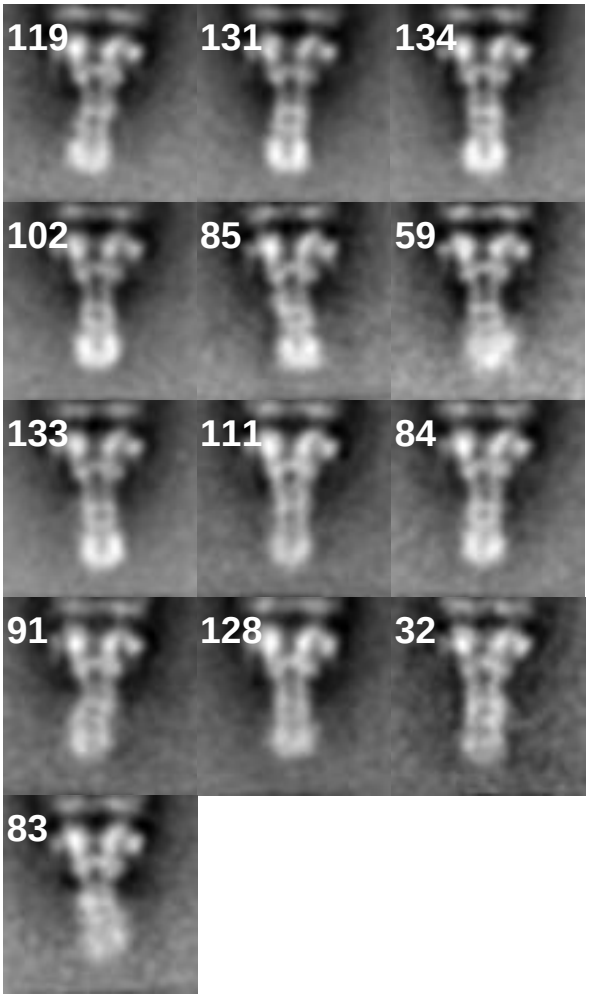

Supplementary Figure 4. Correspondence analysis of GroEL-bound PA pore shows the variability in the positioning of the stem. Stems are bent at the base of the stem or in the middle of the stem in some classes while the cap stays at the same position and orientation.

Supplementary Figure 5

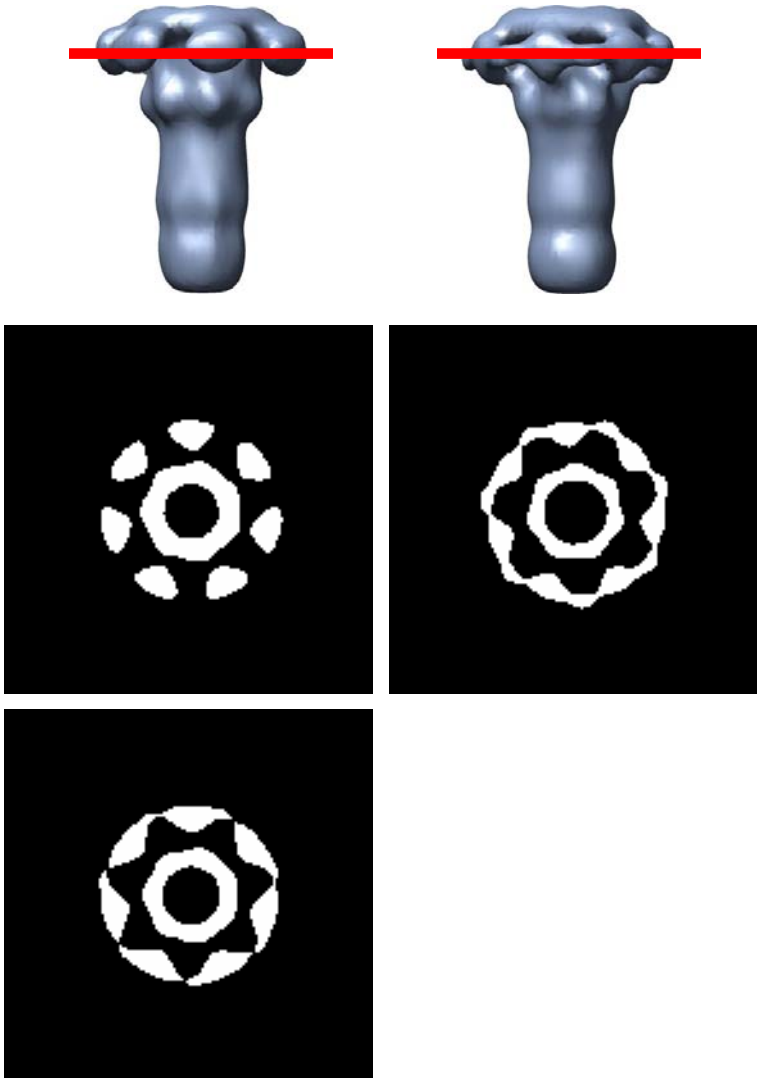

Supplementary Figure 5. 3D reconstruction of GroEL-bound PA pore (Above, left) and free pore (Above, right). Red lines indicate where slices were taken for (Middel, left and right). Middle left, Slice of GroEL-bound PA pore. Middle, right, Slice of free PA pore. Below, Image that is generated with simulated domain 3 movement. Connections between domain 3 of adjacent subunits can be seen. Domain 2 and domain 3 were separately masked out from free pore slice, and reconstituted with random translational movement on domain 3.

Supplementary Figure 6

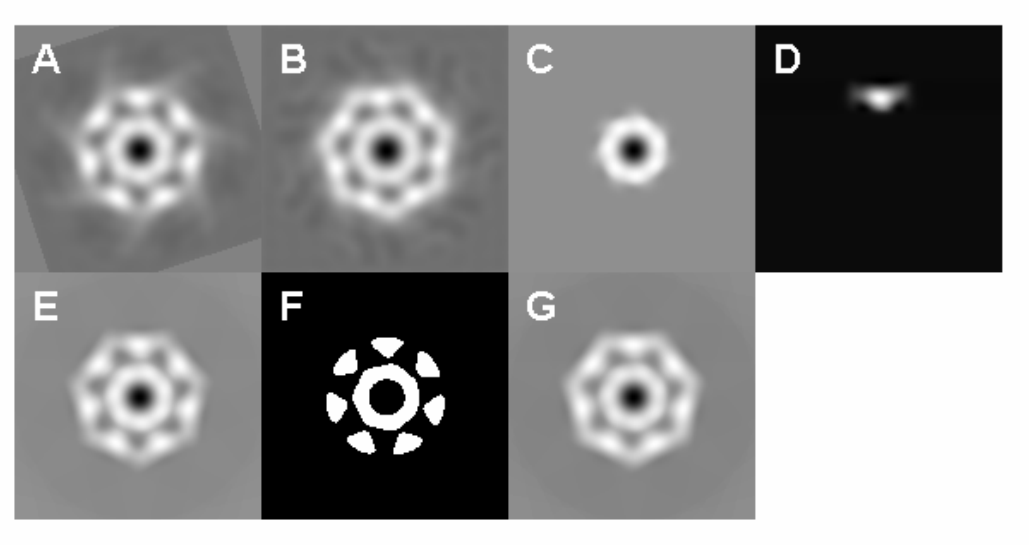

Supplementary Figure 6. (A) A slice of GroEL-bound PA pore reconstruction. (B)A slice of free PA pore reconstruction. (C) Domain 2 was masked out from (A). (D) Domain 3 was masked out from (A). (E) An image which is reconstituted from (C) and (D) closely matches with the original slice (A). (F) When a threshold was set to (E), the image matches exactly to the original slice at the same threshold (Supplementary figure 5). (G) The image was reconstituted from (C) and (D) with random movement on (D).

GroEL as a molecular scaffold for structural analysis of the anthrax toxin pore

Hiroo Katayama[1,5], Blythe E Janowiak[2,5], Marek Brzozowski[1], Jordan Juryck[1], Scott Falke[3], Edward P Gogol[4], R John Collier[2] & Mark T Fisher[1#]

[1] Department of Biochemistry and Molecular Biology, University of Kansas Medical Center, 3901 Rainbow Blvd., KLSIC Building, Kansas City, KS, 66160
[2]Department of Microbiology and Molecular Genetics, Harvard Medical School, Alpert Building, Boston, Massachusetts 02115
[3]Department of Biology William Jewell College, 500 College Hill, Liberty Mo. 64068-1896
[4]School of Biological Sciences, University of Missouri-Kansas City, Kansas City Mo. 64100
[5] These authors contributed equally to this work**.**
[#] Corresponding Author mfisher1@kumc.edu

Supplementary Discussion.

1) Possible origins for β-Barrel Stem Widening.

First, staining artifacts may influence the dimension. In particular, the masking of the bright density at the hydrophobic tip region that was necessary to obtain the structure altered its weight, and hence perhaps its width in the reconstruction. The hollow nature of the stem may have allowed more flattening, widening it in the reconstruction. The stem tip can especially be influenced by negative stain artifacts due to the hydrophobic exterior surface and hydrophilic lumen of the pore. Darker stain inside and lighter stain outside are apparent in the slices of the reconstruction (Supplementary Fig. 2 online), and the light exterior stain density could have contributed to the exaggerated thickness of the stem. A second possible cause for stem widening is the flexibility of this structure, resulting in heterogeneity amongst the particles. Flexibility of the stem region was demonstrated with multivariate statistical analysis and subsequent hierarchical clustering following particle alignment using only the cap (Supplementary Fig. 4 online). As shown, many classes reveal that the stem is bent at different points and to different degrees. The image heterogeneity in the stem region presumably smeared the density, resulting in an apparent thickening of the stem region when seven-fold symmetry was imposed.

2) Possible Origin of the Structural Variability in Free Pore Domain 3.

The binding of GroEL to the pore may constrain the conformational variability of domain 3. To test this hypothesis, we simulated the proposed heterogeneity of the unbound pore. Slices of the free and GroEL-bound pore reconstructions were calculated at the level of the apparent domain 3 contacts (Supplementary Figs. 5, 6). When the data is displayed at a density level corresponding to ~~a~~ 100% of the pore volume, domain 3 of each subunit is free of contacts with adjacent domains 3 in the GroEL-bound pore, while in the free pore structure, each domain 3 is observed making close contact with the adjacent domains 3 (Supplementary Fig. 5). To simulate the proposed conformational freedom of domain 3, portions of domain 2 and domain 3 of GroEL-bound pore that were repositioned with random translations (mean variation = 10 Å) to simulate movement of domain 3 (Supplementary Fig. 6). Averaging these conformations resulted in the appearance of contacts between neighboring domain 3s (Supplementary Fig. 5). Therefore, apparent contacts between adjacent domains in the free pore can be due to conformational flexibility that becomes constrained in the GroEL-bound state.